International Journal of Nanomedicine

Dovepress
open access to scientific and medical research

Open Access Full Text Article

ORIGINAL RESEARCH

Nanoporous diopside modulates biocompatibility, degradability and osteogenesis of bioactive scaffolds of gliadin-based composites for new bone formation

This article was published in the following Dove Press journal:
International Journal of Nanomedicine

Zhaoyu Ba[1,*]
Zhaoxiong Chen[1,*]
Yufeng Huang[1,*]
Du Feng[2]
Qinghui Zhao[3]
Jianguang Zhu[1]
Desheng Wu[1]

[1]Department of Spinal Surgery, Shanghai East Hospital, Tongji University School of Medicine, Shanghai, China; [2]Key Laboratory of Protein Modification and Degradation, School of Basic Medical Sciences, Affiliated Cancer Hospital, Institute of Guangzhou Medical University, Guangzhou Medical University, Guangzhou, China; [3]Biobank, Shanghai East Hospital, Tongji University School of Medicine, Shanghai, China

*These authors contributed equally to this work

Introduction: It is predicted that with increased life expectancy in the whole world, there will be a greater demand for synthetic biomedical materials to repair or regenerate lost, injured or diseased tissues. Natural polymers, as biomedical materials, have been widely applied in the field of regenerative medicine.

Materials and methods: By incorporation of nanoporous diopside bioglass (nDPB) into gliadin (GL) matrix, macro–nanoporous scaffolds of nDPB/GL composites (DGC) were fabricated by method of solution compressing and particles leaching.

Results: The results revealed that the DGC scaffolds possessed well-interconnected macropores of 200–500 μm and nanopores of 4 nm, and the porosity and degradability of DGC scaffolds remarkably increased with the increase in nDPB content. In addition, in vitro cell experiments revealed that the adhesion and growth of MC3T3-E1 cells on DGC scaffolds were significantly promoted, which depended on nDPB content. Moreover, the results of histological evaluations confirmed that the osteogenic properties and degradability of DGC scaffolds in vivo significantly improved, which were nDPB content dependent. Furthermore, the results of immunohistochemical analysis demonstrated that, with the increase in nDPB content, the type I collagen expression in DGC scaffolds in vivo obviously enhanced, indicating excellent osteogenesis.

Discussion and conclusion: The results demonstrated that the DGC scaffolds containing 30 wt% nDPB (30nDGC) exhibited good biocompatibility and new bone formation ability, which might have a great potential for applications in bone regeneration.

Keywords: nanoporous diopside bioglass, gliadin, macro-nanoporous, MC3T3-E1, osteogenesis

Introduction

It is predicted that with increased life expectancy in the whole world, there will be a greater demand for synthetic biomedical materials to repair or regenerate lost, injured or diseased tissues.[1] Natural polymers (eg, collagen, chitosan, starch and cellulose), as biomedical materials, have been widely applied in the field of regenerative medicine.[1–3] As one kind of natural polymer, plant proteins (eg, zein, soy protein and wheat protein [WP]) have gradually attracted more and more attention for biomedical applications, such as cell/tissue culture, drug delivery and tissue regeneration.[4,5] The plant proteins have been shown to have biocompatibility, biodegradability and easy processability to the required shapes that are desirable for biomedical materials. For example, the zein

Correspondence: Desheng Wu
Department of Spinal Surgery, Shanghai East Hospital, Tongji University School of Medicine, 150th Jimo Road, Shanghai 200120, China
Tel +86 189 0189 0240
Email eastspinesci@163.com

submit your manuscript | www.dovepress.com
Dovepress
http://dx.doi.org/10.2147/IJN.S162262

and soy protein have been made into films or electrospun nanofiber scaffolds for biomedical applications.[6,7]

Over the past few years, WPs have been considered for application in regenerative medicine.[8] WP (eg, gliadins [GLs] and glutenins) subunits are linked together by disulfide and hydrogen bonds between cysteine residues to form very large polymers. In addition, the types of amino acid in WP are relatively abundant (eg, glutamate, glycine, proline and serine), which are similar to those of collagen in natural bone.[8] GL has been utilized for industrial applications such as fibers and films.[9] Recently, studies have demonstrated that GL was suitable for biomedical applications, for example, GL films were made into soft capsules and chewable gums for controlled drug release.[10,11] Furthermore, GL nanoparticles have been studied for controlled release of hydrophobic and amphiphilic drugs.[12] Although the GL has good biocompatibility and biodegradability, as a biomaterial for bone tissue repair, the bioactivity of GL needs to be improved to make it practically useable for bone regeneration.[13]

Nanoporous materials have been widely applied as biomaterials for drug loading and releasing, regenerative medicine, etc owing to the unique characteristics including their uniform and tunable pore size distribution, high pore volume and large specific surface area.[14] Compared with the nonporous bioactive glass, the nanoporous bioactive glass possesses higher bioactivity due to its high pore volume and large surface area, thus could accelerate the deposition kinetics of apatite minimization, thereby improving the bioactivity and biocompatibility of the materials.[15] Therefore, as a new class of bioactive material, the nanoporous bioactive glass has a great potential for bone regeneration applications.

Nanocomposite scaffolds containing polymers and nano-bioactive materials (such as hydroxyapatite, bioglass and calcium phosphate) have been shown to have a great potential in regenerative medicine due to their ability to mimic the structural properties of bone tissues of human beings.[16] Development of ideal nanocomposite scaffolds for bone regeneration has revealed the performances of polymer based nanocomposites, which can tailor the desired bioactivity and degradability of the nanocomposite scaffolds with superior biological properties.[17] Moreover, the incorporation of nano-bioactive materials in the polymers offers the required features (biocompatibility and osteoconductivity) that could improve cell adhesion, proliferation and differentiation as well as new bone tissue ingrowth into the scaffolds to ultimately repair bone defects.[18]

The diopside bioceramic has been proven to be biocompatible and bioactive, which has the ability to stimulate the proliferation and osteogenic differentiation of osteoblasts and bone marrow mesenchymal stem cells and promote osteogenesis in vivo.[19] Therefore, in this study, the nanoporous diopside bioglass (nDPB) was fabricated, and macro–nanoporous scaffolds of nDPB/GL composites (DGCs) were developed by incorporation of nDPB into GL matrix. The nDPB possessed improved bioactivity and degradability due to its nanopore, high pore volume and large surface area compared with the nonporous bioactivity materials (eg, bioglass). The influences of nDPB content on biocompatibility, degradability and osteogenic properties of the DGC scaffolds both in vitro and in vivo were investigated.

Materials and methods

Synthesis and characterization of nDPB

The nDPB was synthesized by sol–gel method. Briefly, polyethylene oxide–polypropylene oxide–polyethylen (P123) (4.1 g, molecular weight = 5,800 Da; Sigma-Aldrich Co., St Louis, MO, USA) was dissolved in HCl solution (150 mL, 2 M; Sinopharm Chemical Reagent Co., Ltd., Shanghai, China) with stirring at room temperature for 12 hours. Then, $Ca(NO_3)_2{\cdot}4H_2O$ (4.83 g; Sinopharm Chemical Reagent Co., Ltd.), $Mg(NO_3)_2{\cdot}6H_2O$ (5.25 g; Sinopharm Chemical Reagent Co., Ltd.) and tetraethyl orthosilicate (TEOS, 8.5 mL; Shanghai Lingfeng Chemical Reagent Co., Ltd., Shanghai, China) were dissolved in the aforementioned solution under continuous stirring for 5 hours. The resulting sol-type mixture was placed in an oven for 48 hours at 85°C and then filtrated and washed by deionized water and ethanol for three times, respectively. The collected product was air-dried at 80°C and calcined at 550°C for 6 hours to obtain nDPB powders. The nDPB was characterized by transmission electron microscopy (TEM, JEM-2100; JEOL, Tokyo, Japan) and scanning electron microscopy (SEM, S-4800; Hitachi Ltd., Tokyo, Japan) combined with energy-dispersive spectrometry (EDS). The nitrogen adsorption–desorption isotherms of nDPB were performed by Tristar II 3020 (Micromeritics, Norcross, GA, USA), the pore size distribution was determined by Barrett–Joyner–Halenda (BJH) and the specific surface area was calculated by Brunauer–Emmett–Teller (BET).

Preparation and characterization of DGC scaffolds

GL (50 kD) was purchased from Tokyo Chemical Industry Co., Ltd., Tokyo, Japan. (TCI), and DGC scaffolds with 0 wt%, 15 wt% and 30 wt% nDPB (GL, 15nDGC and 30nDGC) were prepared by a compression method. The weighted GL powders were first dissolved in ethanol solution (analytical reagent, 100%; Shanghai Titan Scientific

Co., Ltd, Shanghai, China), and then nDPB powders with specific weight ratio of GL (0 wt%, 15 wt% and 30 wt%) were added to the abovementioned solution under continuous stirring to obtain the DGCs. Afterwards, the NaCl particles (NaCl/composites = 1:10, weight/weight [w/w]) were added and sufficiently mixed with composites by using a mortar for 1 hour, and the resulting homogeneous mixture (nDPB/GL/NaCl) was obtained. Then, the samples with different sizes (eg, Φ 12 × 2 mm for in vitro tests and Φ 6 × 6 mm for in vivo tests) were prepared by compressing mixture into designed stainless molds under the pressure of 4 MPa. Subsequently, the samples were collected and immersed in deionized water for 24 hours to remove the NaCl, followed by drying at 60°C to get the DGC scaffolds. The scaffolds were characterized by SEM and Fourier transform infrared (FTIR) spectroscopy (Thermo Nicolet 6700; Thermo Fisher Scientific, Waltham, MA, USA). The porosities of the scaffolds (GL, 15nDGC and 30nDGC) were determined by mercury intrusion porosimeter (PoreMaster 60 GT; Quantachrome Instruments, Boynton Beach, FL, USA), which corresponded to a pore diameter range between 3.6 nm and 950 μm.

Degradability, changes in pH and ion concentrations of scaffolds in phosphate-buffered saline (PBS)

The degradability of the scaffolds was determined by evaluating the weight loss ratio of the scaffolds after soaking into PBS solution for different time periods. The samples (Φ 12 × 2 mm) were placed in separate polypropylene vials and incubated in PBS solution (pH = 7.4) at 37°C for 12 weeks. The solution volume/sample weight ratio was 20 mL/g. PBS solution was changed once a week. The samples were taken out at different time points (1, 2, 3, 4, 5, 7, 8, 10 and 12 weeks) from the solution and dried at 40°C in an oven. The percentage of weight loss of the samples was determined as follows:

$$\text{Weight loss}\,(\%) = \frac{\text{Wi} - \text{Wt}}{\text{Wi}} \times 100$$

where Wi and Wt represent the initial weight of the samples and the weight of samples after immersion in PBS solution for different time periods, respectively.

The changes in pH of solution after soaking the scaffolds into PBS for different time periods were monitored by using a pH meter (FE20; Mettler Toledo, Columbus, OH, USA). The concentrations of Ca, Mg and Si ions in PBS solution after soaking 30nDGC scaffolds into PBS for different time periods were detected by inductively coupled plasma atomic emission spectroscopy (ICP-AES; Optima 3000DV; PerkinElmer Inc., Waltham, MA, USA). All experiments were performed in triplicate.

Cell culture

Mouse embryo osteoblast precursor cells (MC3T3-E1; American Type Culture Collection, Manassas, VA, USA) were cultured in 100 mm^2 culture dishes ingrown in Dulbecco's Modified Eagle's Medium (Thermo Fisher Scientific) supplemented with 10% fetal bovine serum (FBS; Altas Biologicals, Dae Myung Science Co., Ltd., Seoul, Korea) and 100 U/mL penicillin and 100 μg/mL streptomycin sulfate (Pen-Strep; Thermo Fisher Scientific). Cultures were incubated at 37°C in a humidified atmosphere of 95% air and 5% CO_2. The culture medium was refreshed every 2 days till 85% of cell confluence, and then the cells were detached by trypsin (0.25%)–EDTA (0.03%) (Thermo Fisher Scientific). The resulting cells were cultured with culture medium in petri dishes. The fourth to sixth passage cells were used for experiments.

Attachment of cells

The samples of GL, 15nDGC and 30nDGC scaffolds (Φ 12 × 2 mm) sterilized by immersing in 100% ethanol for 1 hour and then ultraviolet (UV) radiated for 1 hour were placed in a 24-well plate. The cells were seeded on the scaffolds at a density of 2×10^4 cells/well and incubated for different time periods. After coculture for 6, 12 and 24 hours, the specimens were placed into new 24-well plates, 0.1 mL of the 3-(4,5-dimethylthiazol-2-yl)-2,5-diphenyltetrazolium bromide (MTT) solution (0.5 mg/mL) was added, and then samples were incubated at 37°C. After incubation, 50 μL dimethyl sulfoxide (DMSO; Sinopharm Chemical Reagent Co., Ltd.) was added per well to dissolve the purple formazan and mixed thoroughly by pipetting; the solution was then incubated at 37°C for 10 minutes. The optical density (OD) was measured at 490 nm using an automated plate reader (Synergy HT Multi-Detection Microplate, BioTek Instruments, Inc., Winooski, VT, USA). The results (n = 3) were expressed as OD and converted into percentage; the cell attachment ratio (Ln) was calculated by the following equation:

$$\text{Ln} = \frac{\text{Sn}}{\text{Jn}} \times \frac{\text{Sp}}{\text{Ss}} \times 100\%$$

where Sn is the OD value of the attached cells on scaffolds, Jn is the OD value of the cells on 24-well plates, Ss is the

area of the bottom of 24-well culture plates and Sp is the area of the scaffold surface.

The MC3T3-E1 cells were seeded on the sample surfaces in 24-well culture plates with the density of 2×10^4 cells/well. After culturing for 12 hours, the culture medium was removed, and the samples were washed with PBS solution for three times and fixed with 0.25% glutaraldehyde solution for 30 minutes. Afterward, the fixed cells were progressively dehydrated with a graded series of ethanol solution (10%, 30%, 50%, 70%, 85%, 90% and 100%) for 15 min. Subsequently, the samples with cells were freeze-dried and observed by SEM. All experiments were performed in triplicate.

Cell proliferation and morphology

The proliferation of MC3T3-E1 cells was evaluated by MTT assay. The cells were cultured on the sample surfaces with the density of 2×10^4 cells/sample for 1, 4 and 7 days. At specific time point, the culture medium was replaced with α- MEM (minimum Eagle's medium) (400 μL) and MTT solution (100 μL; Amresco, Dallas, TX, USA) followed by 4 hours of cultivation. After that, the medium was replaced with 500 μL DMSO (Sigma-Aldrich Co.) for 30 minutes. The OD of formazan was measured by microplate reader (AMR-100; Allsheng Co., Ltd., Zhejiang, China) at the wavelength of 490 nm.

Morphology of cells on the scaffolds was investigated after 4 days of culture. The sterilized samples of GL, 15nDGC and 30nDGC scaffolds (Φ 12 × 2 mm) were placed in a 24-well plate. The cells were seeded on the scaffolds at a density of 2×10^4 cells/well and incubated for 4 days. Then, the cells/scaffolds were washed three times with PBS, and cells on the scaffold surfaces were fixed with 4% glutaraldehyde for 2 hours. Finally, the cells/scaffolds were stained with fluorescein isothiocyanate (FITC; Beyotime Biotech, Jiangsu, China) and 4′,6′-diamidino-2-phenylindole (DAPI; Beyotime Biotech) for 40 and 5 minutes, respectively. The morphology of the cells on the samples was observed by confocal laser scanning microscopy (CLSM, Nikon A1R; Nikon Corporation, Tokyo, Japan). All experiments were performed in triplicate.

Osteogenesis of scaffolds in vivo

The animal experiments were performed according to the international standards on experimental animal welfare, and the protocols were reviewed and approved by the animal experiment and care committee of the Ninth People's Hospital affiliated to Shanghai Jiao Tong University School of Medicine, Shanghai, China. The National Institutes of Health guidelines for the care and use of laboratory animals (NIH publication no 85-23 Rev. 1985) were observed. The nine male New Zealand rabbits (2.2–2.5 kg in weight and 3 months in age) were provided by the Laboratory Animal Research Centre of the Ninth People's Hospital affiliated to Shanghai Jiao Tong University School of Medicine and randomly divided into three groups. All the surgeries were performed under general anesthesia achieved via intraperitoneal injection of pentobarbital (20 mg/kg) under sterile conditions. The animals were immobilized supinely, and the hind limbs were shaved, washed and disinfected with 10% povidone iodine. The linear incision (1 cm long) was made on the femoral condyle of each rabbit, exposing the bone surface. The periosteum was dissected from the bone surface, and a bone defect (6 mm in diameter and 6 mm in depth) was created with a trephine bur using a slow-speed drill. To avoid tissue damage due to overheating, 0.9% saline was dripped onto the contact point between the bur and bone. Scaffolds (Φ 6 × 6 mm) were carefully placed into the defects, and the soft tissue above the defect was covered by the skin which was closed with surgical sutures. The rabbits were euthanized at different time periods (1, 2 and 3 months) after surgery, and the femoral condyles containing scaffolds were collected.

Histological analysis

The fixed femoral condyles containing scaffolds (1, 2 and 3 months) were decalcified in 10% EDTA and then embedded in paraffin. Serial sections with a thickness of 5 μm were cut and mounted on polylysine-coated microscope slides. All sections were stained with hematoxylin and eosin (H&E), and a general assessment of the tissue and wound healing was performed using light microscope (Olympus Corporation, Tokyo, Japan). The percentage of new bone area and material residual of each specimen (new bone area and material residual in scaffold/total scaffold area ×100%) was measured by a semiautomatic image analysis system (Image-Pro Plus; Media Cybernetics, Rockville, MD, USA) from each stained histological section.

Immunohistochemical analysis

Monoclonal antibody against human type I collagen antibody was purchased from Sigma-Aldrich Co. Endogenous peroxidase activity was quenched by incubating the tissue sections (1, 2 and 3 months) with 3% H_2O_2 for 20 min before staining with immunoperoxidase. All sections were blocked by 0.1% bovine serum albumin (BSA) with 10% swine serum. Sections were then incubated with the optimal dilution of primary antibody for type I collagen (1:100) overnight at 4°C.

Afterward, sections were incubated with a biotinylated antibody (Dako Denmark A/S, Glostrup, Denmark) for 15 minutes and then incubated with horseradish peroxidase-conjugated avidin–biotin complex (Dako Denmark A/S) for 15 minutes. Antibody complexes were visualized with the addition of a buffered diaminobenzidine substrate for 4 minutes. The reaction was stopped by immersion and rinsing of sections in PBS. Sections were then lightly counterstained with Mayer's hematoxylin and Scott's blue for 40 s each, in between 3 minute rinses with running water. Subsequently, sections were dehydrated with ascending concentrations of ethanol solutions, cleared with xylene and mounted with a coverslip and DePeX mounting medium (BDH Laboratory Supplies, Poole, UK). Then, the sections were observed under a light microscope. The positive expression ratio of type I collagen was calculated by Image-Pro Plus software (Media Cybernetics, Silver Spring, MD, USA) from each histological section.

Statistical analyses

Data were expressed as mean ± SD for all experiments of at least three independent experiments (n = 3) and were analyzed using one-way analysis of variance (ANOVA) with a post hoc test. A p-value of <0.05 was considered statistically significant.

Results

Characterization of nDPB

The SEM micrograph of nDPB is shown in Figure 1A. The nDPB exhibited irregular rod-like particles with the diameter of around 2 μm. The TEM micrograph of nDPB is shown in Figure 1B. The uniform nanoporous channels were found inside the nDPB. Figure 1C shows the EDS of the nDPB and the peaks of Ca, Mg and Si were detected, indicating that the nDPB contained Ca, Mg and Si elements. Figure 1D shows the N_2 adsorption isotherm of nDPB. The type IV curve with an H1 hysteresis loop and a well-defined step at relative pressure (P/P_0) of 0.2–0.4 for nDPB, which was the typical curve of nanoporous material, were found. The nanopore size of the nDPB was around 2 nm, and pore size distribution of nDPB (insert in Figure 1D) was narrow. In addition, the specific surface area and pore volume of nDPB were 870 m^2/g and 0.41 cm^3/g, respectively.

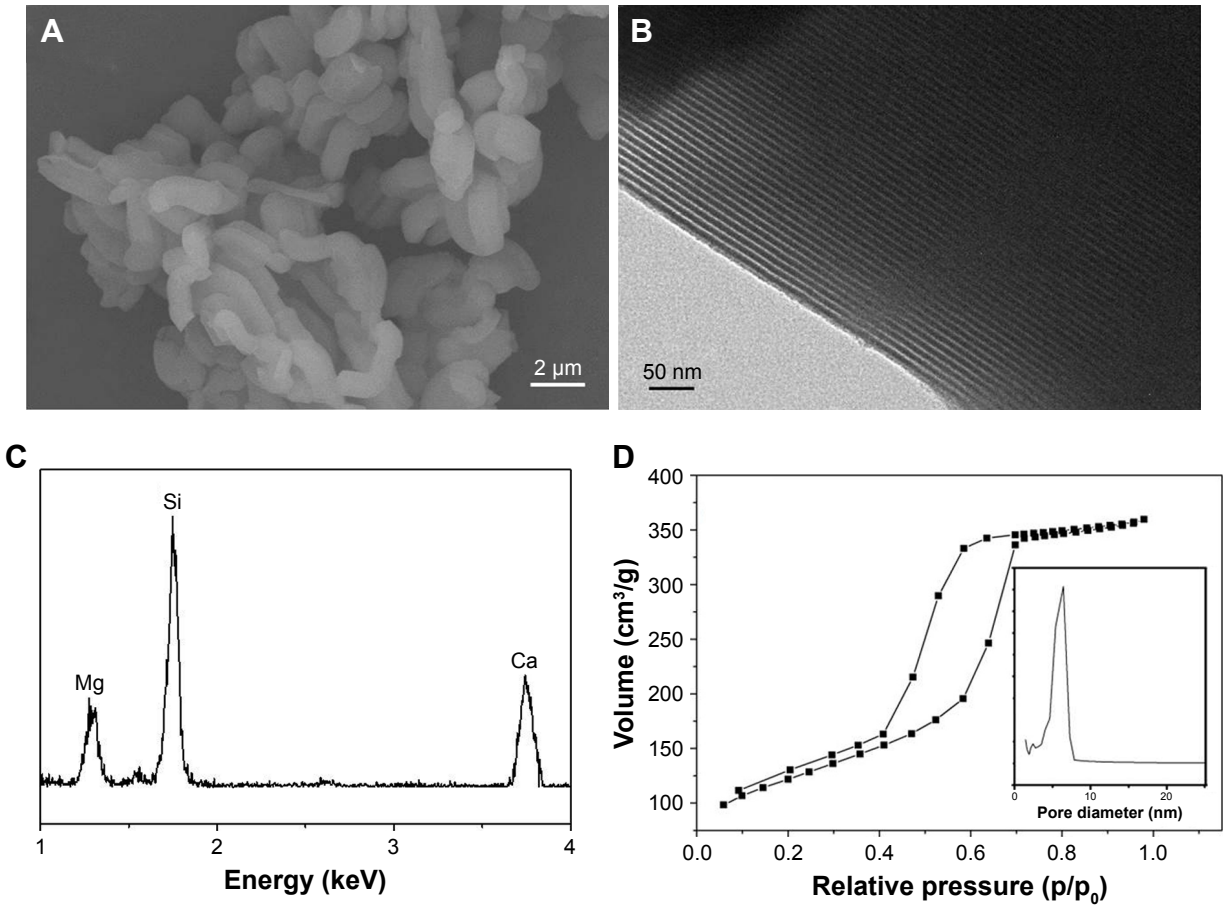

Figure 1 SEM (**A**) and TEM (**B**) micrographs of nDPB, EDS (**C**) of nDPB, and N2 adsorption–desorption isotherms (**D**) of nDPB (pore size distribution insert in **D**).
Note: The magnification of (**A**) is 6.00K, the magnification of (**B**) is 300.00K.
Abbreviations: EDS, energy-dispersive spectrometry; nDPB, nanoporous diopside bioglass; SEM, scanning electron microscopy; TEM, transmission electron microscopy.

Characterization of scaffolds

Figure 2A–F exhibits the SEM micrographs of surface morphology of GL, 15nDGC and 30nDGC scaffolds. It shows that the macropore sizes of the scaffolds ranged from 200 to 500 μm. The porosity of the GL, 15nDGC and 30nDGC scaffolds was 63.4% ± 1.4%, 71.5% ± 1.7% and 80.7% ± 1.1%, respectively. The GL exhibited a smooth pore-wall surface, while both 15nDGC and 30nDGC scaffolds showed the rough pore-wall surfaces. Figure 2G–I shows the EDS mapping of GL, 15nDGC and 30nDGC scaffolds, and dots

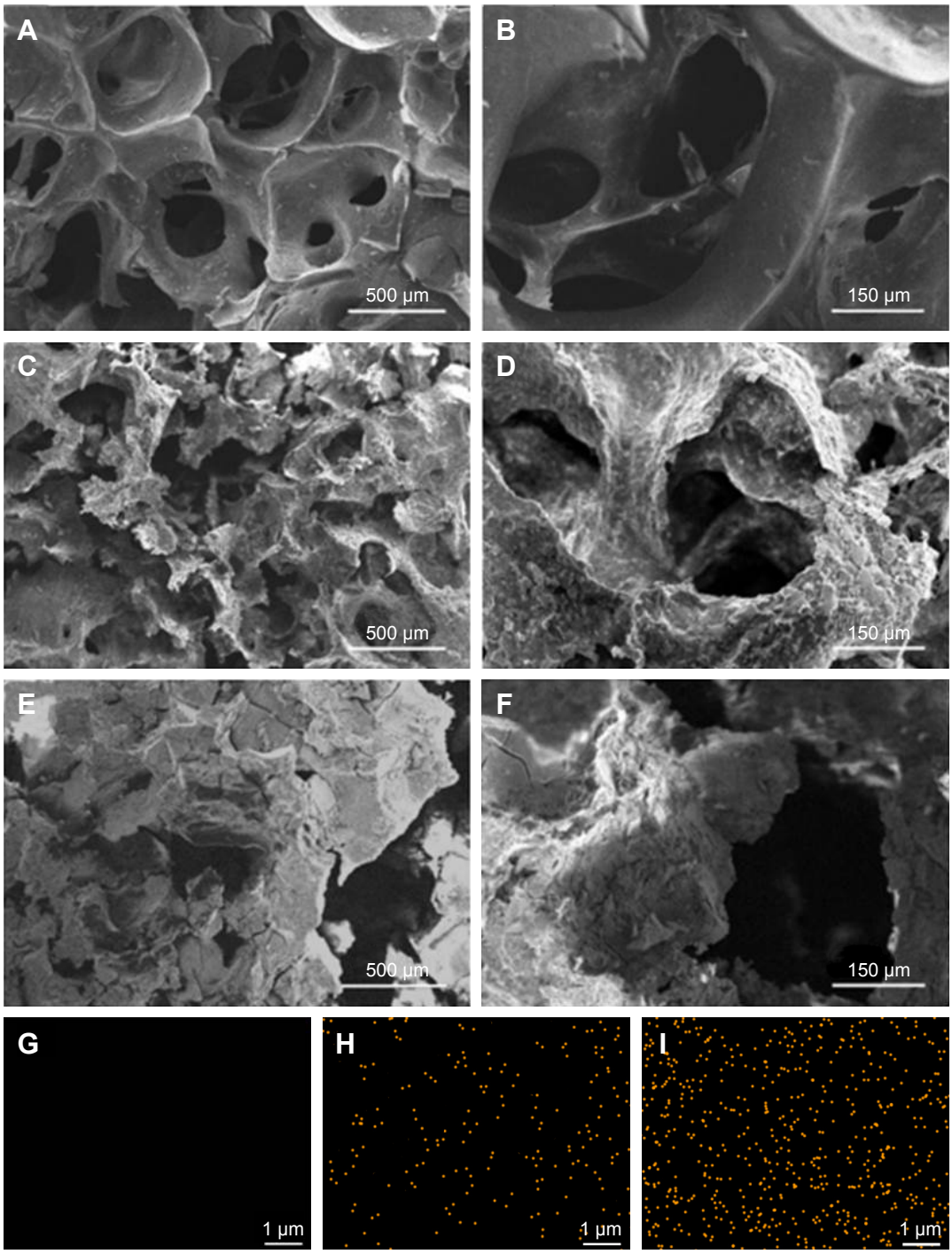

Figure 2 SEM micrographs of surface morphology of GL (**A**, **B**), 15nDGC (**C**, **D**) and 30nDGC (**E**, **F**) scaffolds; EDS mapping of GL (**G**), 15nDGC (**H**) and 30nDGC (**I**), and yellow dots represent Si element, indicating the distribution of nDPB particles into GL.
Note: The magnification of (**A**, **C** and **E**) is ×50, the magnification of (**B**, **D** and **F**) is ×200, the magnification of (**G**, **H** and **I**) is ×10,000.
Abbreviations: EDS, energy-dispersive spectrometry; GL, gliadin; nDPB, nanoporous diopside bioglass; SEM, scanning electron microscopy; 15nDGC, DGC scaffolds with 15 wt% nDPB; 30nDGC, DGC scaffolds with 30 wt% nDPB.

represent Si element (indicating nDPB particles) into GL. It can be seen that the nDPB particles were well distributed into the GL matrix.

Figure 3A exhibits the FTIR spectra of GL, 15nDGC and 30nDGC scaffolds. The characteristic band of GL, at 1,700–1,600 cm^{-1}, corresponded to the –CO–NH– stretching and bending. The peaks at 1,080 and 500 cm^{-1} were found in both 15nDGC and 30nDGC scaffolds, which were attributed to Si–O–Si stretching, indicating the presence of nDPB. Figure 3B shows the weight loss of GL, 15nDGC and 30nDGC scaffolds after immersing in PBS solution for different time periods. The weight loss of GL, 15nDGC and 30nDGC scaffolds increased with time. Moreover, the weight loss of GL, 15nDGC and 30nDGC scaffolds increased with the nDPB content in scaffolds. Figure 3C shows the pH changes of solution after soaking the GL, 15nDGC and 30nDGC scaffolds into PBS for different time periods. The pH of PBS solution containing GL slowly decreased (from 7.4 to 6.70) during the entire 10 days. However, the pH of solution containing 15nDGC (from 7.4 to 7.60) and 30nDGC (from 7.4 to 7.76) scaffolds significantly increased in the first day and then slowly decreased by 6.98 and 7.35 at the 10th day, respectively. Figure 3D shows the changes of Ca, Mg, Si ion concentrations in PBS after soaking 30nDGC scaffolds for different time periods. It could be seen that the concentrations of all ions in solution slowly increased with the increasing immersion time due to the degradation of nDGC.

Cell attachment and growth on scaffolds

Figure 4A reveals the cell attachment ratio of the MC3T3-E1 cultured on GL, 15nDGC and 30nDGC scaffolds for different time periods. Generally, the cell attachment ratio of cells for all samples increased over time. At 6 h, the cell attachment ratio for 30nDGC scaffolds was higher than 15nDGC and GL scaffolds ($p<0.05$). At 12 and 24 hours, the cell attachment

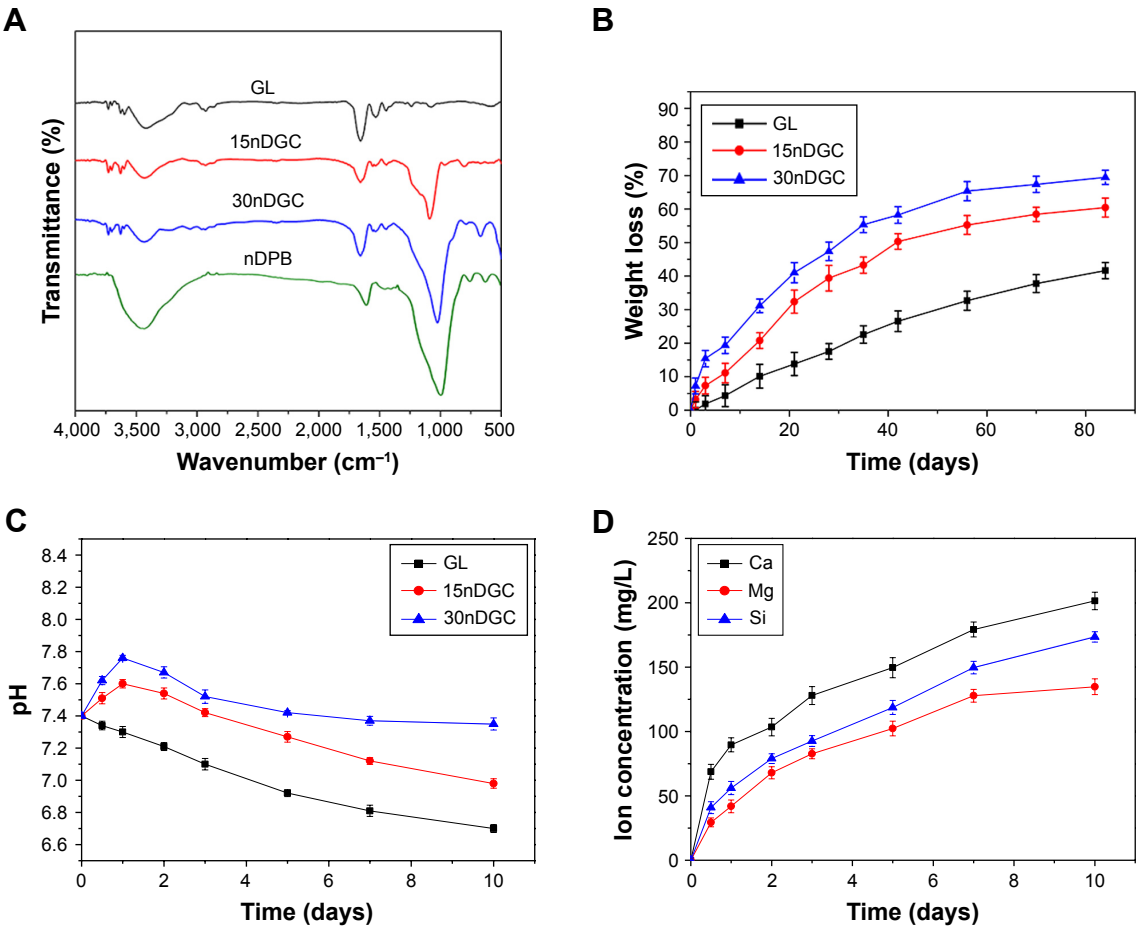

Figure 3 FTIR spectra (**A**) of nDPB, GL, 15nDGC and 30nDGC scaffolds; weight loss (**B**) of the scaffolds after being immersed in PBS solution for different time periods; pH changes (**C**) of solution after soaking the scaffolds in PBS for different time periods; changes of Ca, Mg, Si ion concentrations (**D**) in solution after soaking 30nDGC scaffolds in PBS for different time periods.

Abbreviations: FTIR, Fourier transform infrared; GL, gliadin; nDPB, nanoporous diopside bioglass; PBS, phosphate-buffered saline.

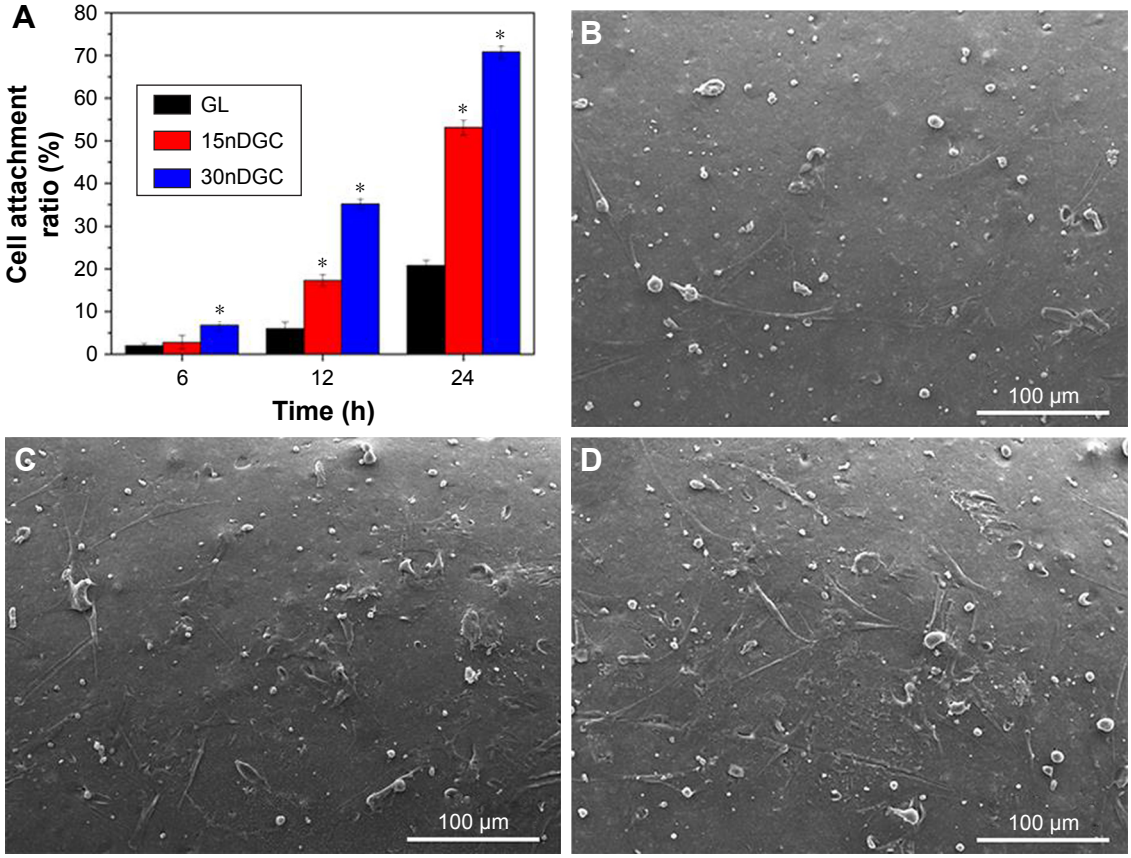

Figure 4 Cell attachment ratio (**A**) of the MC3T3-E1 cells on the scaffolds for 6, 12 and 24 h (*$p<0.05$), SEM images of cells: GL (**B**), 15nDGC (**C**) and 30nDGC (**D**) scaffolds for 12 h.
Note: The magnification of (**B**, **C** and **D**) is ×250.
Abbreviations: GL, gliadin; SEM, scanning electron microscopy.

ratio for 30nDGC scaffolds was significantly higher than 15nDGC scaffolds ($p<0.05$), and 15nDGC scaffolds were remarkably higher than GL scaffolds ($p<0.05$). The SEM micrographs of MC3T3-E1 cells on the scaffolds at 12 hours are shown in Figure 4B–D. It was found that the cells on 30nDGC scaffolds presented an irregular flat morphology with plenty of prominent filopodia. Moreover, more cells attached on 30nDGC scaffold surface than 15nDGC and GL scaffolds, and more cells attached on 15nDGC scaffolds than GL scaffolds.

The OD values (cell proliferation) of MC3T3-E1 cells cultured on the samples for different time periods are shown in Figure 5. The OD values of cells increased with time for all samples, indicating good cytocompatibility. At day 1, the OD values of cells for 30nDGC scaffolds were higher than 15nDGC and GL scaffolds ($p<0.05$). At days 4 and 7, The OD values of cells for 30nDGC and 15nDGC scaffolds were obviously higher than GL scaffolds ($p<0.05$), and 30nDGC scaffolds were higher than 15nDGC scaffolds. The CLSM images of morphology of the MC3T3-E1 cells after being cultured on GL, 15nDGC and 30nDGC scaffolds for 4 days are revealed in Figure 6. A large number of cells were found to attach and grew in all scaffolds, indicating good cytocompatibility. Moreover, the amounts of cells on the scaffolds increased with the nDPB content (30nDGC>15nDGC>GL),

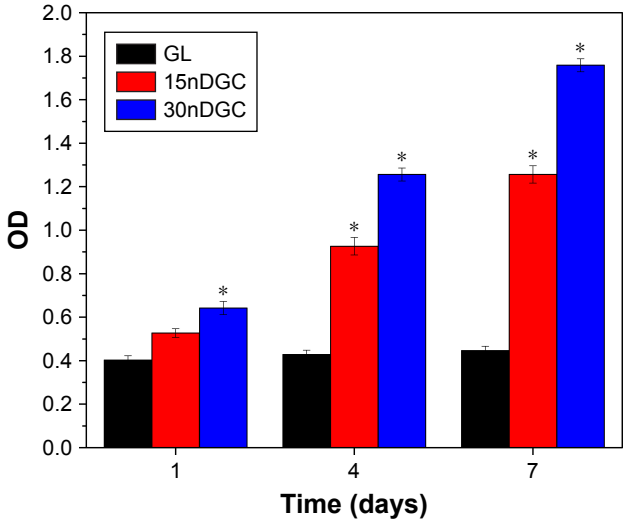

Figure 5 OD values of the MC3T3-E1 cells on GL, 15nDGC and 30nDGC scaffolds for 1, 4 and 7 days, *$p<0.05$.
Abbreviations: GL, gliadin; OD, optical density.

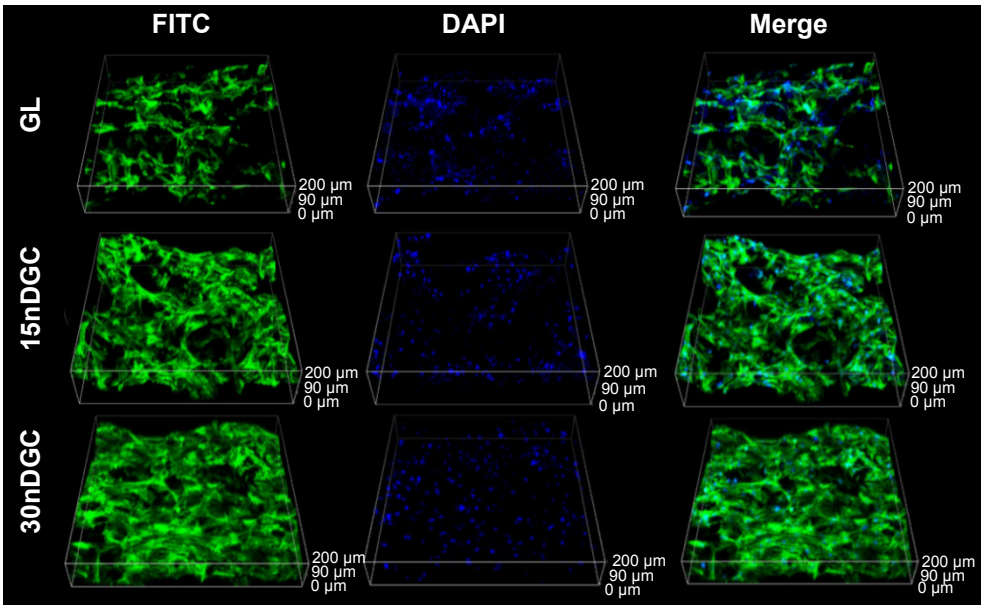

Figure 6 CLSM images of morphology of MC3T3-E1 cells after being cultured on GL, 15nDGC and 30nDGC scaffolds for 4 days.
Abbreviations: CLSM, confocal laser scanning microscopy; DAPI, 4′,6′-diamidino-2-phenylindole; FITC, fluorescein isothiocyanate; GL, gliadin.

indicating that the addition of nDPB into scaffolds promoted the attachment and growth of cells.

In vivo osteogenesis of scaffolds

Histological evaluation

Figure 7 shows the histological sections after the scaffolds implanted in vivo for different time periods. It was found that the new bone tissues in all scaffolds gradually increased with time while the material residual decreased accordingly. Moreover, the NBs in the scaffolds increased with nDPB content in scaffolds, while the material residual decreased accordingly. After implantation for 3 months, more NBs were found in the defects filled with 30nDGC than 15nDGC scaffolds; however, only a few NBs were found in the GL scaffolds (mostly fibrous tissues).

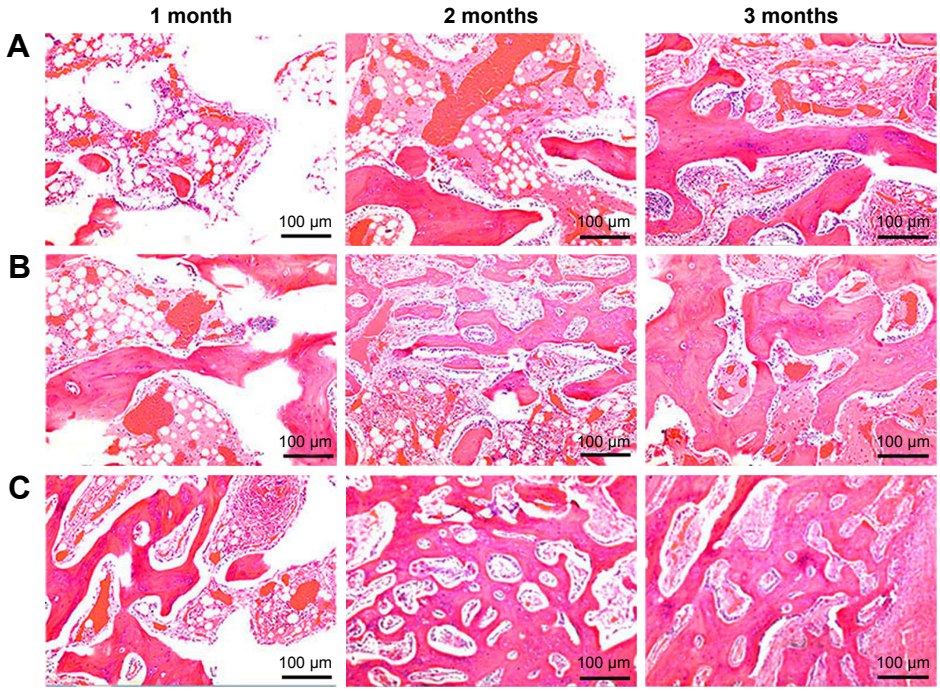

Figure 7 H&E staining of histological sections of GL (**A**), 15nDGC (**B**) and 30nDGC (**C**) scaffolds implanted into femoral defects for 1, 2 and 3 months.
Abbreviations: GL, gliadin; H&E, hematoxylin and eosin.

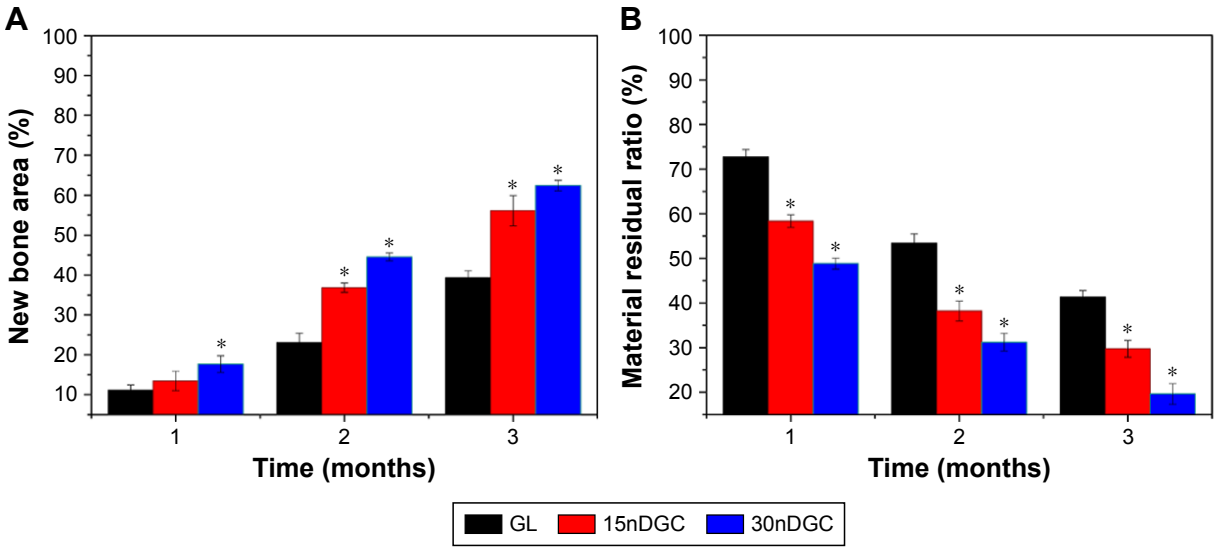

Figure 8 Percentage of new bone area (**A**) and material residual (**B**) after GL, 15nDGC and 30nDGC scaffolds were implanted into femoral defects of rabbits for 1, 2 and 3 months, *$p<0.05$.
Abbreviation: GL, gliadin.

Figure 8 shows the quantitative analysis of new bone area and material residual after the scaffolds implanted in vivo for different time periods. It was found that the new bone area gradually increased with time and nDPB content in scaffolds. At 1 month, the percentage of new bone areas for 30nDGC scaffolds was higher than 15nDGC and GL scaffolds. At both 2 and 3 months, the percentage of new bone areas for 30nDGC and 15nDGC scaffolds were obviously higher than GL scaffolds ($p<0.05$), and 30nDGC scaffolds were obviously higher than 15nDGC scaffolds ($p<0.05$). Accordingly, the percentage of material residual for all scaffolds gradually decreased with time and nDPB content in scaffolds. At both 2 and 3 months, the material residual for 30nDGC and 15nDGC scaffolds was obviously lower than GL scaffolds ($p<0.05$), and 30nDGC scaffolds were obviously lower than 15nDGC scaffolds ($p<0.05$).

Immunohistochemical evaluation

To evaluate the osteogenesis of the scaffolds after implantation in vivo for different time periods, the immunohistochemical of type I collagen staining was conducted. As shown in Figure 9, it was found that the area of type I collagen staining (brown color) in the scaffolds increased with implantation time and nDPB content in the scaffolds (GL<15nDGC<30nDGC).

The quantitative analysis of the expression ratio of type I collagen in the scaffolds is shown in Figure 10. At 1 month, the expression ratio of type I collagen for 30nDGC scaffolds was higher than 15nDGC and GL scaffolds. At month 2, the expression ratio of type I collagen for 30nDGC and 15nDGC scaffolds was obviously higher than GL scaffolds ($p<0.05$). At month 3, the expression ratio of type I collagen for 30nDGC scaffolds was higher than 15nDGC ($p<0.05$), and 15nDGC was higher than GL (GL<15nDGC<30nDGC).

Discussion

Scaffolds for bone regeneration require not only biocompatibility, bioactivity and degradability but also appropriate porous characteristics such as pore size, interconnected pores and porosity, which would benefit cell ingrowth and nutrient delivery.[20,21] In this study, the macro–nanoporous DGC scaffolds with well-interconnected macroporous structures were fabricated by the incorporation of nDPB into GL matrix. The DGC scaffolds possessed not only macropores ranging from 200 to 500 μm (resulting from NaCl particles) but also nanopores with the size of around 4 nm (resulting from nDPB).

Both 30nDGC and 15nDGC scaffolds containing nDPB showed the rough pore-wall surfaces due to the presence of nDPB on the scaffold surfaces, while the GL scaffolds without nDPB exhibited a smooth pore-wall surface. The porosity of GL scaffolds was 63.4%, while the porosity of 15nDGC and 30nDGC scaffolds was 71.5% and 80.7%, respectively. The increase in porosity of the DGC scaffolds was due to the presence of nDPB with nanoporosity, and the nanoporosity of 15nDGC and 30nDGC scaffolds was 8.1% and 17.3%, respectively. The results indicated that the DGC scaffolds contained not only macroporosity but also nanoporosity. It can be suggested that the macroporosity of the scaffolds

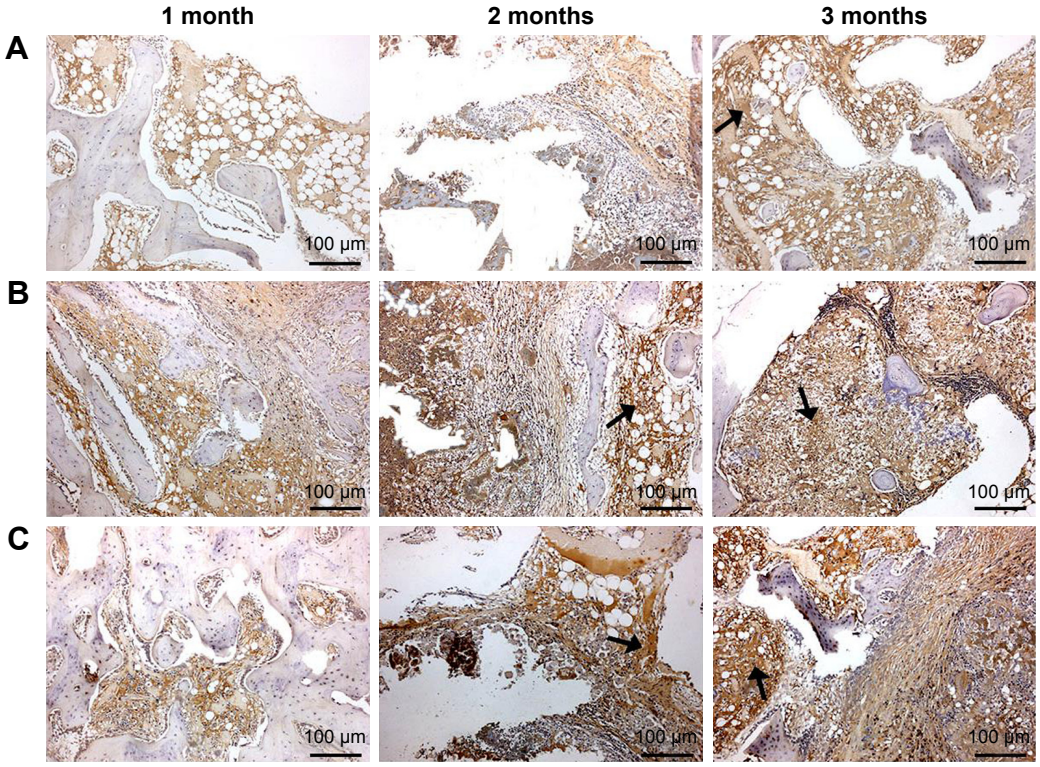

Figure 9 Immunohistological staining of type I collagen after GL (**A**), 15nDGC (**B**) and 30nDGC (**C**) scaffolds implanted into femoral defects of rabbits for 1, 2 and 3 months.
Notes: Arrows represent type I collagen expression. The magnification is ×100.
Abbreviation: GL, gliadin.

could offer sufficient porosity for new bone tissue ingrowth, while the nanoporosity and rough pore-wall surfaces of the DGC scaffolds might have some effects on behaviors and functions of osteoblasts.

Biodegradable scaffolds can provide the initial structure for inducing new bone tissue formation, degrading into new bone tissue forms, providing room for matrix deposition and new bone tissue ingrowth.[22,23] In this study, it was found that the weight loss of the scaffolds in PBS solution gradually increased with the increase in soaking time, indicating that the scaffolds could be degradable. Moreover, the degradability of the scaffolds increased with the nDPB content (30nDGC>15nDGC>GL), indicating that the incorporation of nDPB into GL matrix obviously improved the degradability of the scaffolds. It could also be suggested that the degradation of DGC scaffolds contained the degradation of both nDPB and GL, and the degradability of the nDPB (dissolution of nDPB released Ca, Si and Mg ions into solution) was faster than GL (dissolution of GL released amino acids) due to the presence of nanoporosity in nDPB with huge surface area and high pore volume. The first degradation of nDPB in the scaffolds increased the porosity/pore sizes of the DGC scaffolds (enlarging the surface area of the scaffolds), which would promote the degradability of GL. Therefore, the degradability of the scaffolds increased with the increase in nDPB content.

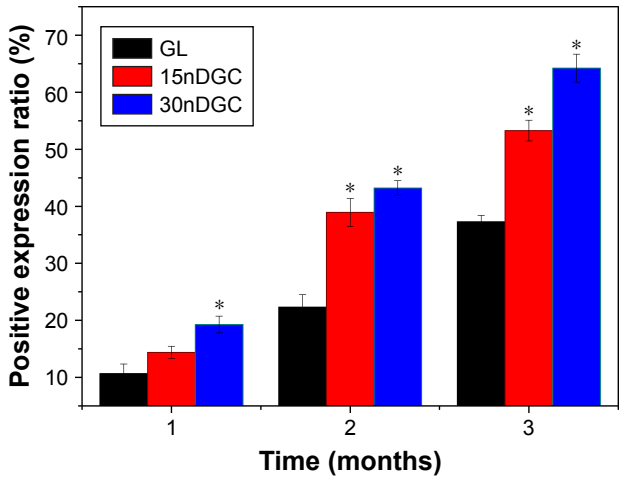

Figure 10 Quantitative analysis of the positive expression ratio of type I collagen after GL, 15nDGC and 30nDGC scaffolds implanted into femoral defects of rabbits for 1, 2 and 3 months, *$p<0.05$.
Abbreviation: GL, gliadin.

The by-products of GL degradation were amino acids, leading to acidic microenvironment, which might be prone to aseptic inflammation in the body.[5,8] In this study, the

pH of the solution for GL decreased slowly from 7.4 to 6.70 during the whole immersion period, indicating that the degradation of GL produced acidic products. As for 15nDGC and 30nDGC scaffolds, the pH increased from 7.4 to 7.60 and 7.76 respective to 15nDGC and 30nDGC in the first 1 day and then showed a slow decrease and stabilized around 6.98 and 7.35 in the following 10 days. The results showed that the degradation of nDPB produced alkaline products, which neutralized the acidic by-products of GL degradation, and the degradation of 30nDGC in solution formed a weak alkaline environment (pH~7.4) similar to biological environment. Therefore, it can be suggested that the 30nDGC scaffolds might be considered as an advantage to avoid possible inflammatory response caused by acidic products of GL degradation, which may be very useful for cell growth/bone formation in vivo.

The initial cell adhesion to the scaffold surface is usually responsible for the ensuing cell spreading and growth on the scaffolds, which is closely correlated with the amounts of new bone formation.[24,25] In this study, the results showed that the adhesion and growth of MC3T3-E1 cells on the DGC scaffolds significantly increased with the increase in nDPB content, and the 30nDGC scaffolds exhibited the highest cell adhesion among these scaffolds. A large number of cells attached and grew into the 30nDGC scaffolds, indicating excellent cytocompatibility. Therefore, it can be suggested that the incorporation of nDPB with good bioactivity into GL obviously promoted the adhesion and growth of the cells on DGC scaffolds (30nDGC>15nDGC>GL). Moreover, the improvement in cell adhesion on 30nDGC scaffolds (containing the highest nDPB content) might be attributed to its rough pore-wall surfaces compared with GL scaffolds with smooth pore-wall surfaces.[26]

Cell proliferation on the biomaterial surface is the second stage of bone remodeling process after cell adhesion, which determines the following cell differentiation and bone formation.[27,28] In this study, the results demonstrated that the 30nDGC scaffolds significantly stimulated the proliferation of the cells compared with 15nDGC and GL scaffolds, indicating that the nDPB content in the scaffolds played a key role in promoting cell proliferation. Previous studies have revealed that the suitable concentrations of Ca, Mg and Si ion release from bioglasses/ceramics (such as diopside) could stimulate the proliferation and differentiation of osteoblasts and bone marrow mesenchymal stem cells.[29,30] In this study, Ca, Mg and Si ions were found to release from the DGC scaffolds. Therefore, it could be suggested that the enhancement of cell proliferation might be attributed to the release of these ions with suitable concentrations (no negative effects on cell growth) due to the degradation of DGC scaffolds, which depended on the nDPB content (30nDGC>15nDGC).

To further evaluate the in vivo osteogenesis, the DGC scaffolds were implanted into the femoral condyles of rabbits. From histological sections after the scaffolds implanted in vivo for different time periods, the results indicated that the newly formed bone tissues in the scaffolds increased with the increase in nDPB content and time. At 3 months after implantation, most of the 30nDGC scaffolds had disappeared (degradation) and the new bone tissues filled most parts of the bone defects. However, although most of the GL scaffolds had disappeared (degradation), the bone defects were filled mostly with fibrous tissues (a few new bone tissues). It can be suggested that compared with GL scaffolds without nDPB, a prominent ingrowth of new bone tissue into 30nDGC scaffolds was achieved due to its relatively high bioactivity (containing nDPB), indicating excellent osteogenesis in vivo.

From the quantitative analysis of new bone area and material residual ratio, the results also indicated that the new bone area gradually increased with the increase in nDPB content, in which the 30nDGC scaffolds possessed the highest percentage of new bone area, indicating that the 30nDGC scaffolds containing the highest nDPB content significantly promoted new bone formation compared with GL. Accordingly, the material residual ratio for the scaffolds gradually decreased with time, in which the 30nDGC scaffolds exhibited the fastest degradability in vivo, indicating that the incorporation of nDPB with nanoporosity into the scaffolds improved the degradability. It is known that the degradation of a biomaterial in vitro can be considered as its dissolution, while the degradation in vivo was affected by both dissolution and cell-mediated degradation.[31] In this study, the results showed that the degradation of the 30nDGC scaffolds in vivo was faster than in vitro. Therefore, the degradation of the 30nDGC scaffolds occurred both chemically (dissolution of both nDPB and GL) and biologically (osteoclast-mediated degradation) in vivo. The first degradation of 30nDGC scaffolds would increase the porosity/pore sizes of the DGC scaffolds, which significantly promoted new bone formation and ingrowth into the scaffolds. Furthermore, the degradation of nDPB released Ca, Si and Mg ions and degradation of GL released amino acids, which would be useful to form new bone in vivo.[12,15]

Type I collagen is the major component of extracellular matrix, which is secreted by osteoblasts at the early stage, and the osteoid matrix deposition is the initial indicator of new bone

formation.[32] In this study, the results of immunohistochemical evaluation of type I collagen expression in the scaffolds by staining and quantitative analysis showed that 30nDGC scaffolds exhibited the highest expression of type I collagen, while the lowest expression was for GL scaffolds, indicating that the 30nDGC scaffolds obviously promoted osteogenesis compared with GL. Therefore, it can be suggested that the nDPB in the scaffolds played key roles for osteoid matrix deposition and new bone formation.

Studies have reported that the osteogenesis of the bioactive scaffolds in vivo is strongly affected by its characteristics, including chemical composition, degradability, bioactivity and pore features (eg, porosity, pore size and pore connectivity).[33,34] In this study, the macro–nanoporous 30nDGC scaffolds containing nDPB had well interconnected macropores of around 300 μm but also nanopores of 4 nm. The content of nDPB in the scaffolds had obviously influences on the bioperformances of the DGC scaffolds, including not only the bioactivity and degradability but also the behaviors and functions of cells and new bone formation ability. In addition, the macroporosity of the 30nDGC scaffolds could offer sufficient porosity for bone tissue growth, while the nanoporosity regulated the osteoblast responses (eg, adhesion and growth). Therefore, the 30nDGC scaffolds with macro–nanoporous structure might be favorable for anchoring and extending cell pseudopods, thus significantly improving cell adhesion, growth and enhanced osteogenesis in vivo.[35] In short, the 30nDGC scaffolds with enhanced bioproperties exhibited the highest new bone formation ability, which has great potential for application in bone tissue engineering.

Conclusion

The DGC scaffolds with macro–nanoporous structures were prepared by the addition of nDPB into GL matrix. The results indicated that the DGC scaffolds containing nDPB possessed not only macroporosity but also nanoporosity. In addition, the porosity and degradability of the DGC scaffolds were remarkably improved with the increase in nDPB content. Moreover, compared with GL scaffolds, the attachment and growth of MC3T3-E1 cells on the DGC scaffolds were obviously promoted, which depended on nDPB content. Furthermore, the results of in vivo evaluation indicated that the DGC scaffolds containing nDPB significantly promoted new bone formation accompanying the scaffolds gradual degradation in vivo. The results demonstrated that the addition of nDPB into GL significantly improved the biological performances (biocompatibility, degradability and osteogenesis) of the DGC scaffolds, and the 30nDGC scaffolds have great potential for applications in bone regeneration.

Acknowledgment

This work was supported by grants from the National Natural Science Foundation of China (81371994), Youth Talent Support Program from Shanghai East Hospital and the Key Discipline Construction Project of Pudong Health Bureau of Shanghai (PWZxk2017-08).

Disclosure

The authors report no conflicts of interest in this work.

References

1. Qazi TH, Mooney DJ, Pumberger M, Geissler S, Duda GN. Biomaterials based strategies for skeletal muscle tissue engineering: existing technologies and future trends. *Biomaterials*. 2015;53:502–521.
2. Wang X, You C, Hu X, et al. The roles of knitted mesh-reinforced collagen-chitosan hybrid scaffold in the one-step repair of full-thickness skin defects in rats. *Acta Biomater*. 2013;9(8):7822–7832.
3. Eftekhari S, El SI, Bagheri ZS, Turcotte G, Bougherara H. Fabrication and characterization of novel biomimetic PLLA/cellulose/hydroxyapatite nanocomposite for bone repair applications. *Mat Sci Eng C Mater*. 2014;39:120–125.
4. Zhou PY, Xia Y, Cheng XS, Wang PF, Xie Y, Xu SG. Enhanced bone tissue regeneration by antibacterial and osteoinductive silica-HACC-zein composite scaffolds loaded with rhBMP-2. *Biomaterials*. 2014;35(38):10033–10045.
5. Mandal BB, Grinberg A, Gil ES, Panilaitis B, Kaplan DL. High-strength silk protein scaffolds for bone repair. *Proc Natl Acad Sci U S A*. 2012;109(20):7699–7704.
6. Zhang Z, Hu J, Ma PX. Nanofiber-based delivery of bioactive agents and stem cells to bone sites. *Adv Drug Deliv Rev*. 2012;64(12):1129–1141.
7. Tutak W, Sarkar S, Lingibson S, et al. The support of bone marrow stromal cell differentiation by airbrushed nanofiber scaffolds. *Biomaterials*. 2013;34(10):2389–2398.
8. Feng SP, Li JY, Jiang XS, et al. Influences of mesoporous magnesium silicate on the hydrophilicity, degradability, mineralization and primary cell response to a wheat protein based biocomposite. *J Mater Chem B*. 2016;4:6428–6436.
9. Kuktaite R, Newson WR, Rasheed F, et al. Monitoring nanostructure dynamics and polymerization in glycerol plasticized wheat gliadin and glutenin films: relation to mechanical properties. *ACS Sustain Chem Eng*. 2016;4:2998–3007.
10. Balaguer MP, Gavara R, Hernandez-Munoz P. Food aroma mass transport properties in renewable hydrophilic polymers. *Food Chem*. 2012;130:814–820.
11. Gulfam M, Kim JE, Lee JM, Ku B, Chung BH, Chung BG. Anticancer drug-loaded gliadin nanoparticles induce apoptosis in breast cancer cells. *Langmuir*. 2012;28(21):8216–8223.
12. Duclairoir C, Orecchioni AM, Depraetere P, Osterstock F, Nakache E. Evaluation of gliadins nanoparticles as drug delivery systems: a study of three different drugs. *Int J Pharm*. 2003;253(1–2):133–144.
13. Joye IJ, Davidov-Pardo G, Ludescher RD, McClements DJ. Fluorescence quenching study of resveratrol binding to zein and gliadin: towards a more rational approach to resveratrol encapsulation using water-insoluble proteins. *Food Chem*. 2015;185:261–267.
14. Guo F, Schulte L, Vigild ME, Ndoni S. Load-release of small and macromolecules from elastomers with reversible gyroid mesoporosity. *Soft Matter*. 2012;8:11499–11507.

15. Liu YZ, Li Y, Yu XB, Liu LN, Zhu ZA, Guo YP. Drug delivery property, bactericidal property and cytocompatibility of magnetic mesoporous bioactive glass. *Mater Sci Eng C*. 2014;41:196–205.
16. Kikuchi M, Itoh S, Ichinose S, Shinomiya K, Tanaka J. Self-organization mechanism in a bone-like hydroxyapatite/collagen nanocomposite synthesized in vitro and its biological reaction in vivo. *Biomaterials*. 2001; 22(13):1705–1711.
17. Liu Y, Meng H, Konst S, Sarmiento R, Rajachar R, Lee BP. Injectable dopamine-modified poly(ethylene glycol) nanocomposite hydrogel with enhanced adhesive property and bioactivity. *ACS Appl Mater Interfaces*. 2014;6(19):16982–16992.
18. Garg T, Singh O, Arora S, Murthy R. Scaffold: a novel carrier for cell and drug delivery. *Crit Rev Ther Drug Carrier Syst*. 2012;29(1):1–63.
19. Tsigkou O, Jones JR, Polak JM, Stevens MM. Differentiation of fetal osteoblasts and formation of mineralized bone nodules by 45S5 Bioglass conditioned medium in the absence of osteogenic supplements. *Biomaterials*. 2009;30(21):3542–3550.
20. Sleep E, Cosgrove BD, Mcclendon MT, et al. Injectable biomimetic liquid crystalline scaffolds enhance muscle stem cell transplantation. *Proc Natl Acad Sci U S A*. 2017;114(38):E7919–E7928.
21. Gershlak JR, Hernandez S, Fontana G, et al. Crossing kingdoms: using decellularized plants as perfusable tissue engineering scaffolds. *Biomaterials*. 2017;125:13–22.
22. Correia C, Bhumiratana S, Yan LP, et al. Development of silk-based scaffolds for tissue engineering of bone from human adipose derived stem cells. *Acta Biomater*. 2012;8:2483–2492.
23. Dorj B, Won JE, Purevdorj O, et al. A novel therapeutic design of microporous-structured biopolymer scaffolds for drug loading and delivery. *Acta Biomater*. 2014;10(3):1238–1250.
24. Pina S, Oliveira JM, Reis RL. Natural-based nanocomposites for bone tissue engineering and regenerative medicine: a review. *Adv Mater*. 2015; 27(7):1143–1169.
25. Gao CD, Peng SP, Feng P, Shuai CJ. Bone biomaterials and interactions with stem cells. *Bone Res*. 2017;5:17059.
26. Mehl C, Kern M, Schutte AM, Kadem LF, Selhuber-Unkel C. Adhesion of living cells to abutment materials, dentin, and adhesive luting cement with different surface qualities. *Dent Mater*. 2016;32(12):1524–1535.
27. Kang H, Chen H, Huang P, et al. Glucocorticoids impair bone formation of bone marrow stromal stem cells by reciprocally regulating microRNA-34a-5p. *Osteoporos Int*. 2016;27(4):1493–1505.
28. Shuai CJ, Feng P, Wu P, et al. A combined nanostructure constructed by graphene and boron nitride nanotubes reinforces ceramic scaffolds. *Chem Eng J*. 2017;313:487–497.
29. Zhai WY, Lu HX, Wu CT, et al. Stimulatory effects of the ionic products from Ca-Mg-Si bioceramics on both osteogenesis and angiogenesis in vitro. *Acta Biomater*. 2013;9(8):8004–8014.
30. Tian T, Han Y, Ma B, Wu CT, Chang J. Novel Co-akermanite (Ca2CoSi2O7) bioceramics with the activity to stimulate osteogenesis and angiogenesis. *J Mater Chem B*. 2015;3:6773–6782.
31. Arulmoli J, Wright HJ, Phan DTT, et al. Combination scaffolds of salmon fibrin, hyaluronic acid, and laminin for human neural stem cell and vascular tissue engineering. *Acta Biomater*. 2016;43:122–138.
32. Ben Shoham A, Rot C, Stern T, et al. Deposition of collagen type I onto skeletal endothelium reveals a new role for blood vessels in regulating bone morphology. *Development*. 2016;143(21):3933–3943.
33. Wang C, Lin K, Chang J, Sun J. Osteogenesis and angiogenesis induced by porous β-CaSiO(3)/PDLGA composite scaffold via activation of AMPK/ERK1/2 and PI3K/Akt pathways. *Biomaterials*. 2013; 34(1):64–77.
34. Gao CD, Feng P, Peng SP, Shuai CJ. Carbon nanotubes, graphene and boron nitride nanotubes reinforced bioactive ceramics for bone repair. *Acta Biomater*. 2017;61:1–20.
35. Wu ZY, Zheng K, Zhang J, et al. Effects of magnesium silicate on mechanical property, biocompatibility, bioactivity, degradability, osteogenesis of poly(butylene succinate) based composite scaffolds for bone repair. *J Mater Chem B*. 2016;4:7974–7988.